Supplementary information

Supplementary methods

Patients

Patient 1 is a 14-year-old Caucasian boy with intellectual disability, autism, attention deficit hyperactivity disorder (ADHD), dyskinesias, hallucinations and congenital adrenal hyperplasia. He developed choreiform movements of both upper and lower extremities, hand tremors and orobuccollingual dyskinesia at 5 years of age. He was treated with risperidone which did not improve his involuntary movements. He had seizure-like activity characterized by whole body shaking and unresponsiveness after he was treated with risperidone, but his EEG was always normal, also during such episodes. He nevertheless received valproate and topiramate which were not helpful. Valproate worsened his hand tremor. With topiramate, he developed hallucinations and a significant cognitive decline. After risperidone, valproate and topiramate were discontinued, his seizure like activities stopped. He has hyperreflexia (especially of the lower extremities), reduced muscle tone and cogwheeling at the wrists. He has an aggressive behavior and limited speech, social interactions and adaptive skills. Brain MRI revealed a few prominent perivascular spaces bilaterally and a small non-specific hyperintense T2 and FLAIR signal in the left centrum semiovale. Whole exome sequencing revealed the *de novo SCN8A* c.4859G>T, p.R1620L mutation (called R1620L throughout), and biallelic point mutations in the *CYP21A2* gene (p.V282L and p.I173N).

Patient 2 is a 23-months-old girl with mixed African American and Caucasian background who presented at 10 months with developmental delay, hypotonia, absent reflexes, myopathy, fasciculations and chorea-like movements, growth failure, and vomiting. Brain MRI showed mild unspecific bilateral parietal periventricular white matter FLAIR hyperintensities. Extensive genetic and biochemical testing has been non-diagnostic. Her family history is unremarkable. She has never experienced any seizures and an EEG has

never been performed. Whole exome sequencing revealed the *de novo SCN8A* c.4865C>A, p.A1622D mutation (called A1622D throughout).

Patient 3 is a 15-month-old Caucasian boy with an epileptic encephalopathy and severe hypotonia. He was born after an uneventful pregnancy and uncomplicated vaginal birth at term. He had his first seizure lasting a few minutes at his 3rd day of life. At day 7, seizures recurred and within the first two months of life he was hospitalized 2-3 times per month due to status epilepticus. At 15 months of age he has medically intractable generalized seizures 2-3 times per week. All seizures have arisen from sleep with a semiology of tonic posturing of all extremities, teeth chenching, cyanosis and a tonic upward gaze. The duration of seizures was between 5 and 90 minutes. Since the age of 14 months, he has constantly been whining/crying between seizures. As anti-epileptic drugs he was first treated with levetiracetam with an add-on of vigabatrin and rufinamide. When the diagnosis was evident, levetiracetam was replaced by oxcarbazepine. Currently he is initiating treatment with phenytoin. Furthermore, treatment with gabapentin and chloral hydrate was initiated for the discomfort. Ketogenic diet led to seizure aggravation and a trial of pyridoxal-5 phosphate was attempted with no effect. At the age of 15 months he had normal eye contact, truncal hypotonicity and did not sit independently. There was a short period with failure to thrive when he was 5 weeks old where a nasogastric tube was inserted, but at age 8 weeks full breast-feeding was resumed. Investigations included a normal brain MRI and lumbar puncture, including infectious titers, amino acids and neurotransmitters. EEG showed a normal background, multifocal paroxysmal interictal sharp wave activity in the temporo-frontal regions bilaterally. Ophthalmological examination was normal apart from a discrete immature left optic nerve. Gene panel testing revealed the *de novo SCN8A* mutation c.5614C>T, p.R1872W (called R1872W throughout).

Patient 4 is a 10 months old Caucasian girl with onset of focal seizures at 4.5 months of age. She was born after an uneventful pregnancy and uncomplicated vaginal birth at term. She presented with focal seizures

evolving into secondary generalized tonic-clonic seizures (duration 3-4 min), occurring either during sleep, or when falling asleep/waking up. Interictal EEG was normal. During the course of the disease the seizure frequency increased to one seizure every fourth hour. She was initially treated with levetiracetam and topiramate, however, due to the increased seizure frequency, clobazam was added which led to seizure reduction, but resulted in developmental regression which improved again when clobazam was tapered off. When the diagnosis was evident, oxcarbazepine was added. At the age of 10 months, she is developing normally, has reached all developmental milestones and has currently been seizure-free for three months. Gene panel testing revealed the *de novo SCN8A* mutation c.4423G>A, p.Gly1475Arg. Apart from this one relatively mild case, we have been collecting several more cases carrying the G1475R with well treatable epilepsy and only mild ID that will be reported elsewhere.

Patient 5 was a 10 weeks old girl. Her mother noticed seizures already in utero, and the girl elicited seizures from 1st day of life. Seizures were tonic, focal dyscognitive as well as high frequency hypertonic myoclonias. Seizures occured both during wake and sleep. Seizures remained refractive, despite having tried several different AEDs, including phenobarbital, levetiracetam, lacosamide, phenytoin (initial response but not on a longer term), vigabatrine and sultiam. However, vigabatrin and clobazam had a positive effect on the myoclonias. An initial EEG showed burst suppression with sharp waves on the right side, and a follow-up EEG has shown low amplitudes with multifocal sharp waves. MRI was normal. Developmentally, the girl has never gained any basic skills. She suffered from hypotonia and cortical blindness. She died in a non-treatable convulsive status epilepticus. Gene panel testing revealed the *de novo SCN8A* mutation c.5280G>A, p.Met1760Ile.

Exome sequencing for patients 1 and 2 was performed by Ambry Genetics. Gene panel testing for patients 3, 4 and 5 was performed at Amplexa Genetics or at CeGaT GmbH. All genetic studies were performed with

informed consent of the patients or their responsible relatives and were approved by the local ethical committees.

Primary neuronal cultures

The pregnant mice were cervically dislocated after asphyxiation by CO_2, the embryos were taken out and decapitated immediately. The hippocampi within the whole brain stored in cold magnesium- and calcium-free HBSS solution (PAA Laboratories GmbH) were recognized under the dissecting microscope (Olympus SZ 61, Shinjuku, Tokyo, Japan) and isolated using fine forceps. After three times washing with cold HBSS solution, the hippocampal tissue was incubated for 14 min in 2.5% trypsin (Invitrogen) at 37°C and then washed by DMEM with FCS to block the enzyme digestion. Dissociated neurons were obtained by gentle mechanical trituration and plated on 13-mm coverslips in 24-well culture plates filled with 500 µl DMEM supplemented with FCS and penicillin/streptomycin (Invitrogen). The coverslips were coated with poly-D-lysine prior to the embryo preparation. After six hours, during which neurons could settle on the cover slips in 5% CO_2 humidified atmosphere at 37°C, the culture medium was replaced by Neurobasal culture medium (Invitrogen) supplemented with B27 (Invitrogen), glutamine, and penicillin/streptomycin.

Immunohistochemistry

Cultured hippocampal neurons from which we recorded were filled with 0.5% biocytin and – after the recording – fixed for 15 min with 4% paraformaldehyde. After washing steps with 0.3% Triton X-100 in PBS, neurons were incubated for 4 h at room temperature or overnight at 4°C with Cy3-conjugated streptavidin (Sigma Aldrich, dilution 1: 667) in PBS containing 0.3% Triton X-100. The remaining streptavidin was removed by extensive washing steps with PBS. Blocking was performed in 10 mM Tris solution supplemented with 0.15 M NaCl, 0.1% Triton X-100 and 4% nonfat milk powder for 1 h at room

temperature. Neurons were incubated with a monoclonal chicken antibody against GFP (Millipore Bioscience, dilution 1:2000) or a monoclonal rabbit antibody against GFP (Invitrogen, dilution 1:300) combined with a monoclonal mouse antibody against GAD67 (Millipore Bioscience Research Reagents, dilution 1:500) or a monoclonal chicken antibody against MAP2 (Abcam, dilution 1:2000) for 1 h at room temperature. After washing steps with blocking solution, neurons were incubated for 1 h at room temperature with a secondary Alex Fluor 488-conjugated goat anti-chicken antibody (Invitrogen, dilution 1:500) or a secondary Alex Fluor 488-conjugated goat anti-rabbit antibody (Invitrogen, dilution 1:500) combined with an Alex Fluor 568-conjugated goat anti-mouse antibody (Invitrogen, dilution 1:500) or an Alex Fluor 647-conjugated goat anti-chicken antibody (Invitrogen, dilution 1:500). DAPI (Sigma Aldrich, dilution 1:5000) was used to identify the nuclei. After washing steps with PBS, the coverslips plated with neurons were air-dried and mounted with a mounting medium (Southern Biotech) prior to examination under an Axiovision2 plus Zeiss microscope (Jena, Germany).

Data analysis

The activation curve (conductance–voltage relationship) was derived from the current–voltage relationship that was obtained by measuring the peak current at various step depolarizations from the holding potential of -100 mV according to:

$$g(V) = \frac{I}{V - V_{rev}}$$

with g being the conductance, I the recorded peak current at the test potential V, and V_{rev} the apparent observed Na^+ reversal potential. Boltzmann function:

$$g(V) = \frac{g_{max}}{1 + exp\left[\left(V - V_{1/2}\right)/k_v\right]}$$

with g being the conductance, I the recorded current amplitude at test potential V, V_{rev} the Na^+ reversal potential, g_{max} the maximal conductance, $V_{1/2}$ the voltage of half-maximal activation and k_V a slope factor.

Steady-state inactivation was determined using 100-ms conditioning pulses to various potentials followed by the test pulse to -10 mV at which the peak current reflected the percentage of non-inactivated channels. A standard Boltzmann function was fit to the inactivation curves:

$$I(V) = \frac{I_{max}}{1 + exp\left[\left(V - V_{1/2}\right)/k_v\right]}$$

with *I* being the recorded current amplitude at the conditioning potential *V*, I_{max} being the maximal current amplitude, $V_{1/2}$ the voltage of half-maximal inactivation and k_V a slope factor.

To determine the time constants of fast inactivation, the cell membrane was depolarized to various test potentials from a holding potential of -100 mV to record Na^+ currents. A second-order exponential function was fit to the time course of fast inactivation during the first 70 ms after onset of the depolarization, yielding two time constants. The weight of the second slower time constant was relatively small. Only the fast time constant, named τ_h, was therefore used for data presentation in the 'Results' section.

Recovery from fast inactivation was recorded from holding potentials of -100 mV. Cells were depolarized to -20 mV for 100 ms to inactivate all voltage-gated Na^+ channels and then repolarized to -80 mV or -100 mV for increasing duration followed by a second depolarizing pulse to -20 mV for 5 ms. A first-order exponential function with an initial delay was fit to the time course of recovery from inactivation yielding the time constant τ_{rec} except for the A1622D mutation, for which a second-order exponential function with an initial delay was used. The $\tau_{rec\ fast}$ of A1622D mutation, which represents the component with the larger amplitude, was compared to τ_{rec} of WT.

Computational modelling

We used a single-compartment conductance-based model

$$C_m\dot{V} = I_{in} - I_L - I_{Na} - I_K,$$

with injected current I_{in}, leak current $I_L = \overline{g}(V - E_L)$, sodium current $I_{Na} = \overline{g}_{Na} m^3 h(V - E_{Na})$ and

potassium current $I_K = \overline{g}_K n^4 (V - E_K)$, each with its maximum ionic conductances $\overline{g}_i$ and ionic reversal potential E_i. The dynamics of the gating variables h, n evolved according to

$$\phi_x \tau_x (V - x_{shift}) \dot{x} = x_\infty (V - x_{shift}) - x,$$

with steady state activation/inactivation curve $x_\infty(V)$, time constant$\tau_x(V)$, a scaling factor ϕ_x for the time constant of the respective gating variable ($\phi_h = 0.2,\ \phi_n = 0.2$) and a shift parameter x_{shift} ($m_{shift} =$ 0mV, $h_{shift} = 0$mV, $n_{shift} = 0$mV). The sodium activation variable was assumed to be instantaneous with $m = m_\infty (V - m_{shift})$. A mininum value for h could be set to enable a persistent current ($h_{persist} = (1 - h_{min}) \cdot h + h_{min}$). We used the parameter settings from Wang and Buzsáki (Wang and Buzsáki, 1996), who described a single compartment model for hippocampal interneurons.

To model the effect of the A1622D mutation on the spike shape of a transfected hippocampal neuron we slowed the Na^+ channel inactivation by setting $\phi_h = 10$. The case without TTX was modeled by adding an unaltered WT Na^+ current and scaling the conductances accordingly: $I_{Na,noTTX} = 0.6 \cdot I_{Na,wt} + 0.4 \cdot I_{Na,slowed}$. To observe effects of other parameter changes, we performed additional simulations with these three models with either $m_{shift} = 3$ mV, $h_{shift} = 20$ mV, $h_{min} = 0.08$ or these three changes combined. We would like to emphasize, that we used this model to qualitatively demonstrate that firing can be modified by such gating changes in a way we observed in transfected neurons. The model and the implemented changes of gating parameters do not quantitatively reflect the measured results from our experiments. Instead, we adjusted the values of the parameter changes modeling the effects of the mutation such that the resulting firing behavior roughly matched the recorded data. As an example, a $m_{shift} = 7$ mV, as observed experimentally for the A1622D mutation, resulted in a model, which could not fire APs. Also, the specific ratio of $I_{Na,wt}$ and $I_{Na,slowed}$ was chosen as the one that described the observed firing behavior best. The modeling was done with custom software written in Python 3.5. Numerical integration was performed with the Euler forward method with a step size of 0.01 ms.

Supplementary reference

Wang XJ, Buzsáki G. Gamma oscillation by synaptic inhibition in a hippocampal interneuronal network model. J. Neurosci. 1996; 16: 6402–13.

Supplementary figures

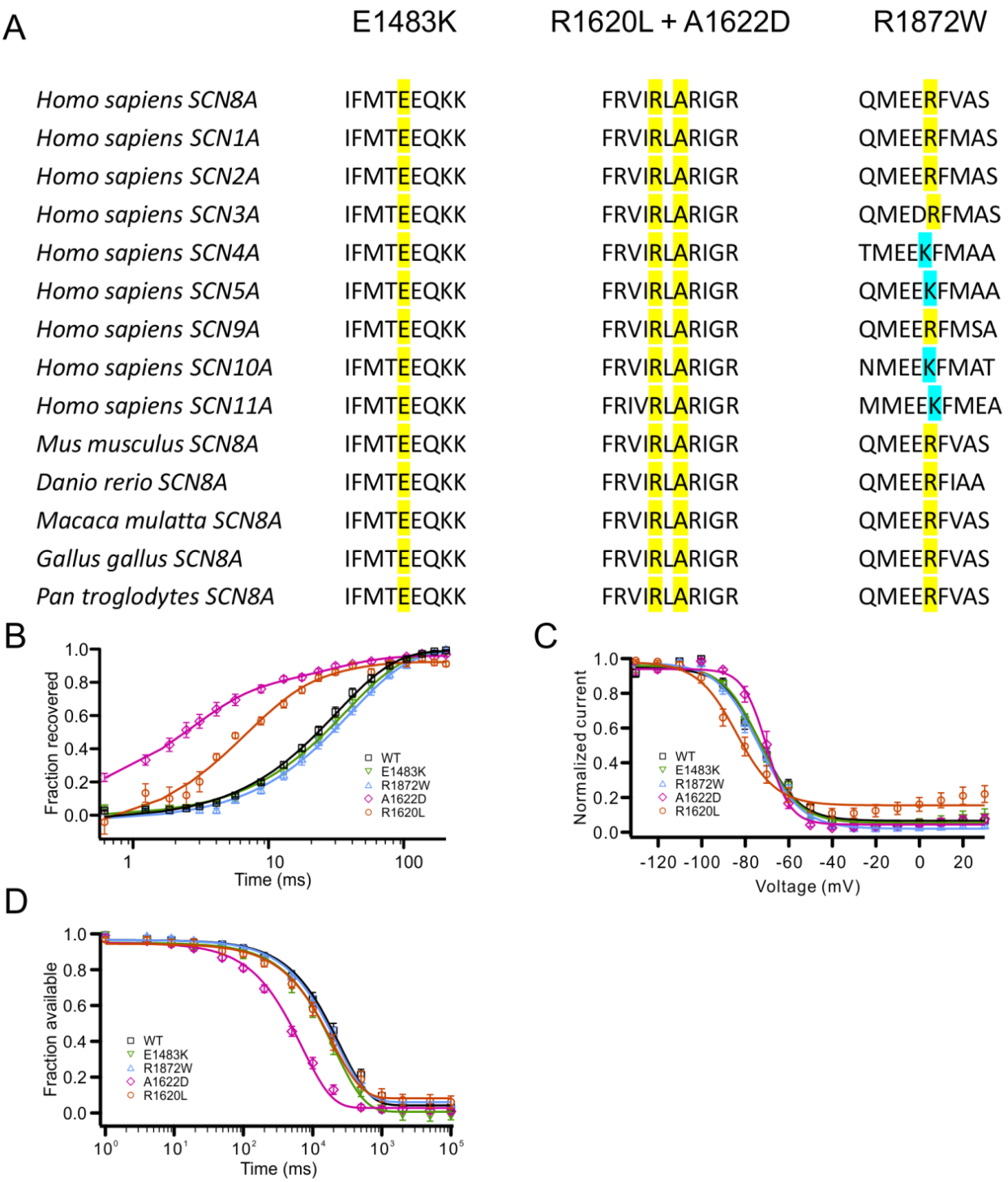

Supplementary Figure 1 Conservation of all four SCN8A mutations and further selected biophysical properties of $Na_V1.6$ mutant channels in ND7/23 cells. (**A**) The alignment analysis shows that all four *SCN8A* mutations and the surrounding amino acids are highly evolutionarily conserved. (**B**) Time course of recovery from fast inactivation at -80 mV: A first- or a second-order exponential function (second-order only for the A1622D mutation; the amplitude of the fast component was 50 ± 2%, of the slow component 25

± 1%, and of the offset 23 ± 1%) with an initial delay was fit to the data points. Both A1622D and R1620L mutations accelerated the recovery from fast inactivation compared to the WT (WT, τ_{rec} = 30.7 ± 2.2 ms, n = 22; A1622D, $\tau_{rec\ fast}$ = 2.4 ± 0.2 ms, n = 22, *** p < 0.001; R1620L, τ_{rec} = 7.3 ± 0.7 ms, n = 14, ** p < 0.01; ANOVA on ranks with Dunn´s posthoc test). (**C**) Steady-state slow inactivation. A standard Boltzmann function was fit to the data points. The A1622D mutation increased the slope of the steady-state slow inactivation compared to the WT (WT, k = 8.4 ± 0.5, n = 9; A1622D, k = 4.7 ± 0.3, n = 7; ** p < 0.01, ANOVA on ranks with Dunn´s posthoc test) and the R1620L mutation caused a hyperpolarizing shift of the steady-state slow inactivation compared to WT (WT, $V_{1/2}$ = -72.0 ± 2.0 mV, n = 9; R1620L, $V_{1/2}$ = -83.0 ± 2.7 mV, n = 6; * p < 0.05, ANOVA on ranks with Dunn´s posthoc test). The E1483K and R1872W mutations did not cause a significant change of steady-state slow inactivation. (**D**) Entry into slow inactivation. The lines represent fits of a first-order exponential function to the data points. Only the A1622D mutation significantly accelerated the entry into slow inactivation in comparison with WT (WT, τ_{entry} = 2663 ± 335 ms, n = 9; A1622D, τ_{entry} = 728 ± 69 ms, n = 10, *** p < 0.001, ANOVA on ranks with Dunn´s posthoc test).

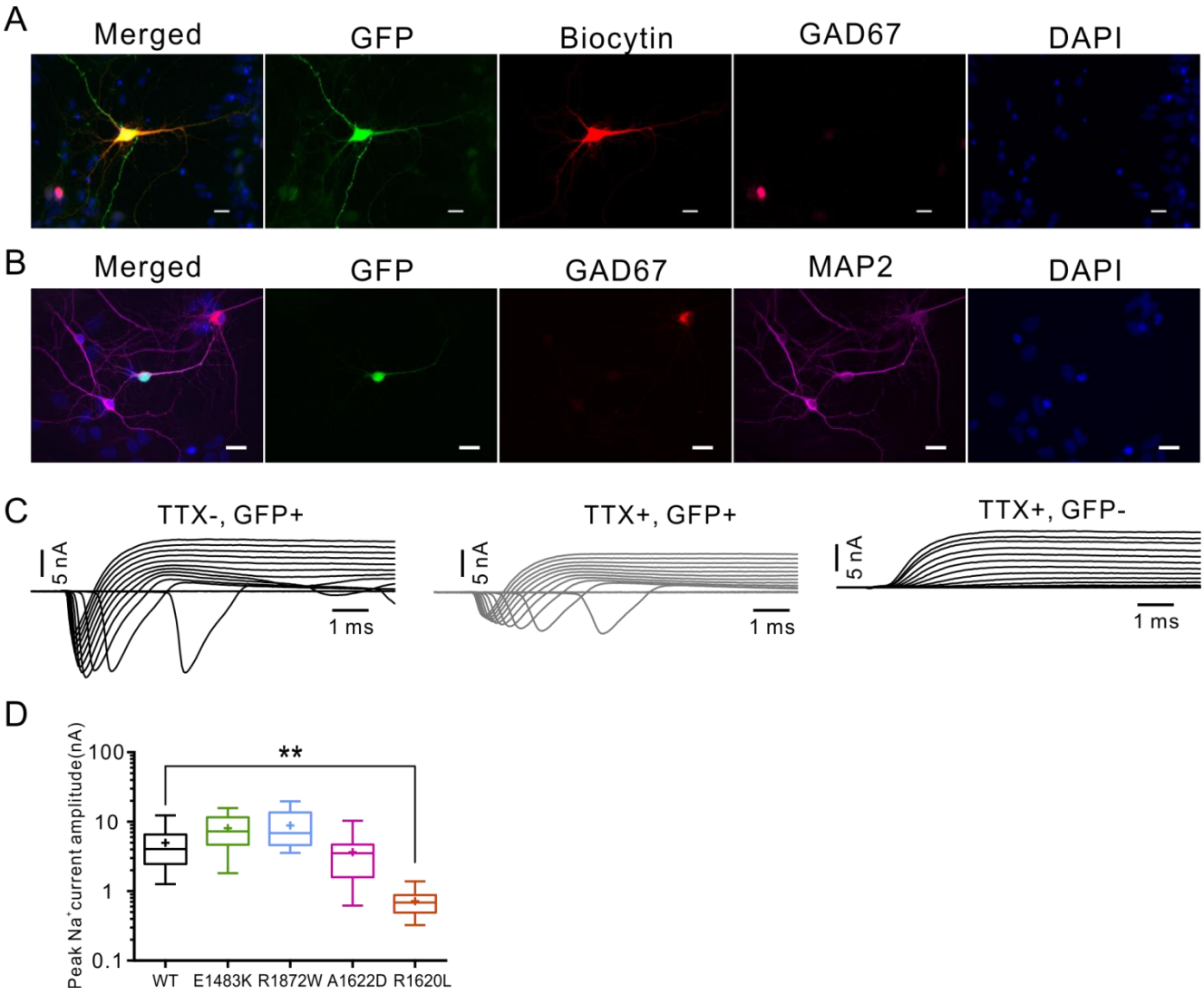

Supplementary Figure 2 Immunostaining and Na^+ current of transfected hippocampal neurons. (**A**) A transfected hippocampal neuron, which was recorded and filled with biocytin, was stained with a monoclonal anti-GFP antibody (green fluorescence), with Cy3-conjugated streptavidin (red fluorescence), a monoclonal anti-GAD67 antibody (purple fluorescence) and DAPI (blue fluorescence). The picture indicates that the transfected neuron is not an inhibitory neuron. Scale bar: 20 μm. (**B**) Immunostaining of transfected hippocampal neurons are shown with a green fluorescence for co-transfected GFP as in (A), but a red fluorescence now indicates GAD67, the marker for inhibitory neurons, and a purple fluorescence for MAP2 (a neuronal marker), plus the blue fluorescence for DAPI to show the nucleus. Scale bar: 20 μm. (**C**) Transfected neurons were recognized by the green fluorescence of the co-transfected enhanced green fluorescent protein (GFP). In the absence of tetrodotoxin (TTX), the transfected neuron exhibited a robust

Na^+ current up to 15 nA carried by both endogenous and transfected sodium channels. After applying TTX, the sodium current amplitude, which was then only carried by transfected TTX-resistant Na^+ channels, was reduced to 7 nA. The GFP-negative, i.e. non-transfected neuron did not exhibit any Na^+ current in the presence of TTX which blocked all endogenous Na^+ channels. The shapes and delays of the fast Na^+ currents after membrane depolarization indicate severe space clamp artefacts, so that these recordings were only used to estimate the current amplitudes. (**D**) Peak Na^+ current amplitudes of transfected neurons in the presence of TTX are presented as boxplots showing the means (plus sign), the 25th, 50th and 75th percentiles, minima and maxima on a logarithmic scale. Only the R1620L mutation caused a significant reduction of the Na^+ current amplitude compared to the WT. ** $p < 0.01$, ANOVA on ranks with Dunn´s posthoc test.

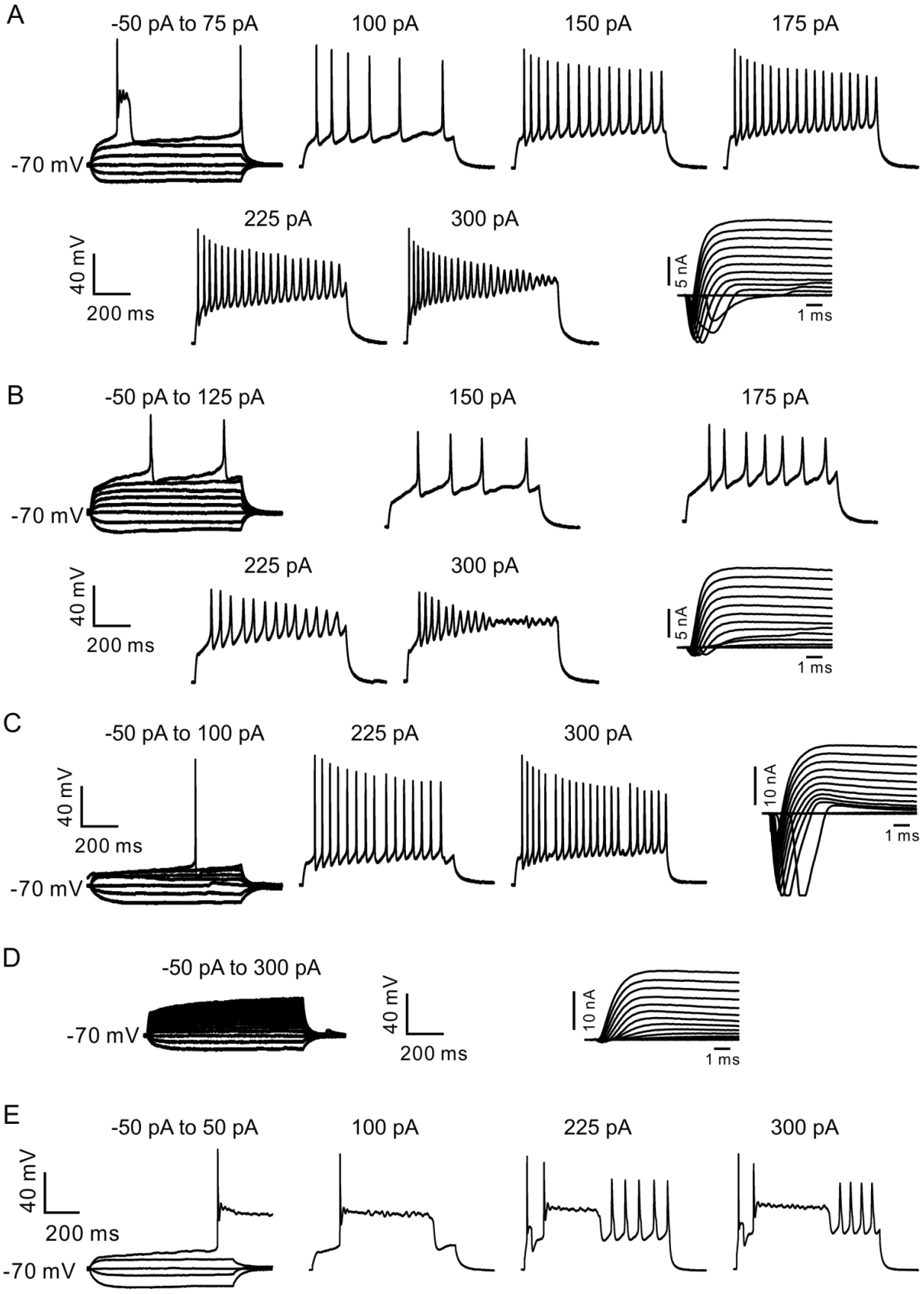

Supplementary Figure 3 Variability of AP firing in neurons transfected with A1622D mutant Na^+ channels. (**A**, **B**) Single APs elicited plateau currents with a depolarization block in a neuron transfected

with A1622D mutant channels in the absence of TTX (**A**) and no depolarization block in the presence of TTX (**B**). The neuron exhibited 8.2 nA peak Na^+ current in the absence of TTX (**A**) and 1.4 nA peak Na^+ current in the presence of TTX (**B**). (**C**, **D**) Regular AP firing in a neuron transfected with A1622D mutant channels in the absence of TTX (**C**) and no AP in the presence of TTX (**D**). The neuron exhibited more than 20 nA Na^+ current in the absence of TTX (**C**). After TTX applying, it exhibited 0.6 nA Na^+ current (**D**), which was not sufficient to generate AP firing. (**E**) Long-lasting depolarization blocks in a neuron transfected with A1622D mutant channels in the absence of TTX. Shown are recordings of voltage responses upon a series of current injections ranging from -50 pA to 300 pA with 25 pA increments of representative cells. Ten out of 19 recorded cells showed such a depolarization block in the absence of TTX, and 7 out of 12 cells in the presence of TTX.

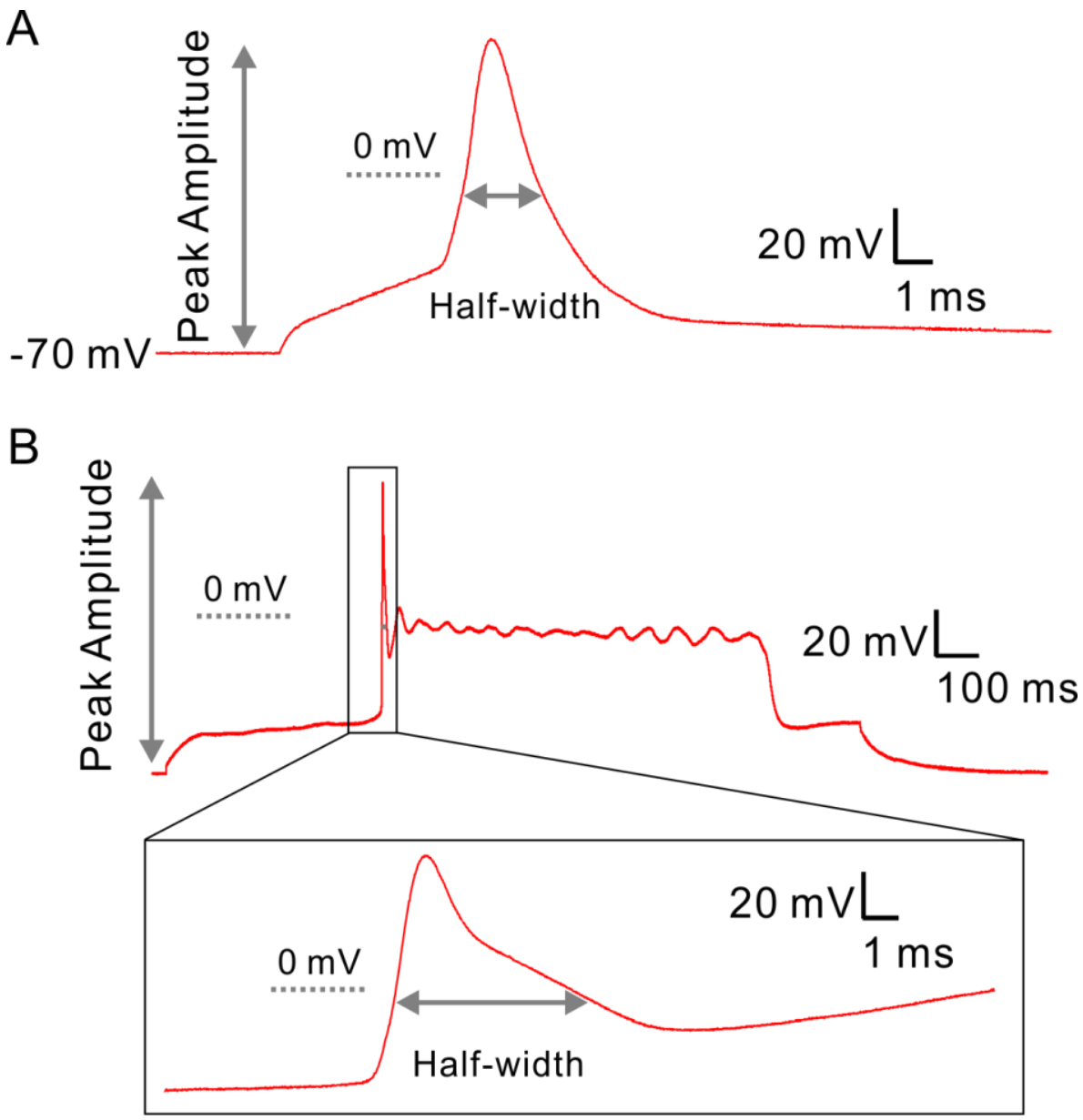

Supplementary Figure 4 Determination of the peak amplitude and the half-width of single APs. (**A**) The peak amplitude was measured from the base line (at -70mV) to the peak of the spike. The half-width was determined when 50% of the peak amplitude was reached during the repolarization process. (**B**) Example to determine the peak amplitude and the half-width of the first AP in a neuron transfected with A1622D mutant channels. Although the A1622D mutation caused a plateau of the single AP, the plateau did not influence the half-width of a single AP (shown in the inset with higher time resolution).

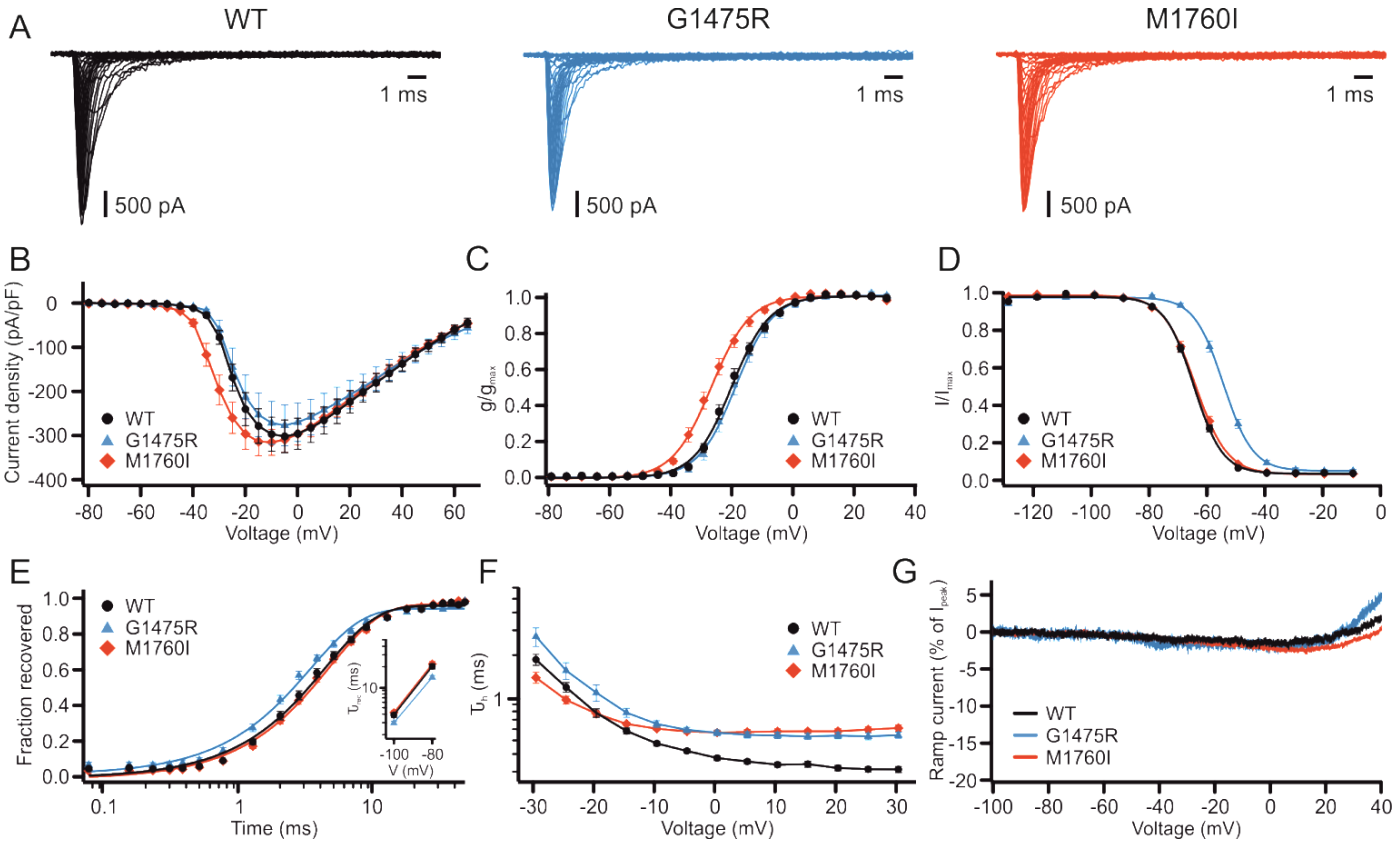

Supplementary Figure 5 Functional studies of two more *SCN8A* mutations in ND7/23 cells. (**A**) Representative Na^+ current traces from *SCN8A* WT (black), G1475R (blue) and M1760I (red) respectively. (**B**) Peak Na^+ currents normalized by cell capacitances were plotted versus voltage. The M1760I mutation (red) caused a left-shift of the current-voltage relationship. WT, n = 23; G1475R, n = 16; M1760I, n = 21. (**C**) Voltage-dependent steady-state activation curves. Lines represent Boltzmann functions fit to the data points. (**D**) Voltage-dependent steady-state inactivation curves. Lines represent Boltzmann functions as in (**C**). (**E**) Time course of recovery from fast inactivation at -100 mV. The inset shows mean values of the recovery time constant at two different voltages. The G1475R mutation accelerated the recovery from fast inactivation compared to the WT. (**F**) Voltage-dependence of the major time constant of fast inactivation τ_h. (**G**) Averaged ramp currents upon ramp stimuli from -100 to +40 mV lasting 800 ms. WT, n = 18; G1475R, n = 14; M1760I, n = 19. Shown are means ± SEM (**B**-**F**).

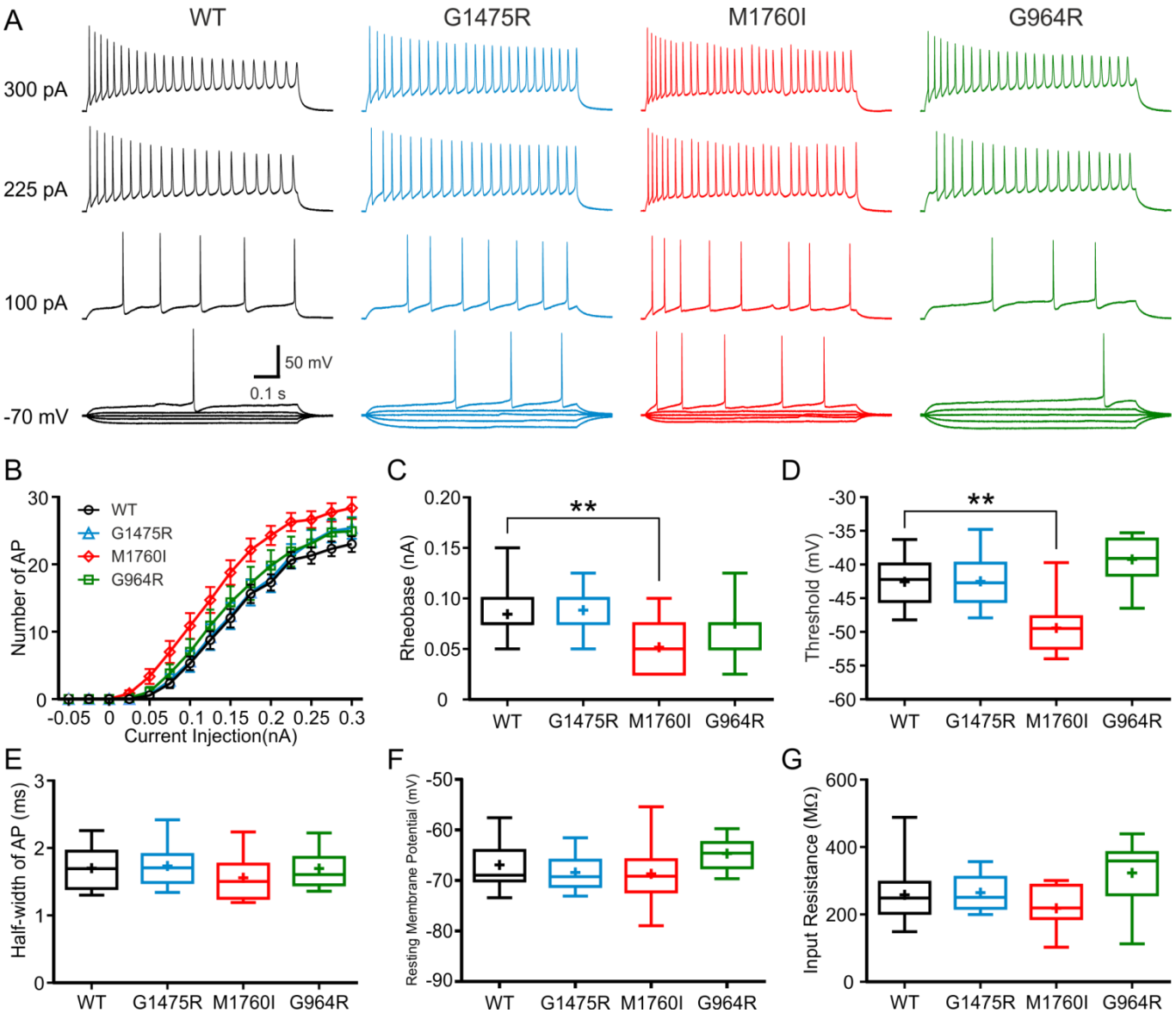

Supplementary Figure 6 Neuronal consequences of three more SCN8A mutations in primary cultured hippocampal mouse neurons. Neurons were transfected with human WT or mutant $Na_V1.6$ channels. Intrinsic neuronal and firing properties were recorded in the absence of TTX. (**A**) Representative voltage traces of evoked action potentials (APs) recorded in the current clamp mode for neurons transfected with WT, G1475R, M1760I, or G964R channels, respectively. (**B**) Number of APs plotted versus injected current. Shown are means ± SEM for each data point (WT, n = 16; G1475R, n = 15; M1760I, n = 14; G964R, n = 11). The area under the curve was determined for each neuron over the whole range of current injections, the value for the M1760I mutation was significantly enhanced compared to WT but not changed for other

mutations. (**C** and **D**) Rheobase (minimal injected current to elicit an AP) (**C**) and Threshold (**D**) of neurons transfected with WT or mutant channels. Only transfection of M1760I mutant channels significantly reduced the rheobase and threshold compared to the WT channels. (**E**) Half-width of single APs was not altered by mutant channels. (**F** and **G**) Resting membrane potentials (**F**) and input resistances (**G**) were not significantly different between neurons transfected with WT or mutant channels. Box-and-whisker plots (**C**-**G**) show means (plus sign), the 25^{th}, 50^{th} and 75^{th} percentiles, minima and maxima; ** $p < 0.01$; one-way ANOVA with Dunnett´s posthoc test or ANOVA on ranks with Dunn´s posthoc test were performed.

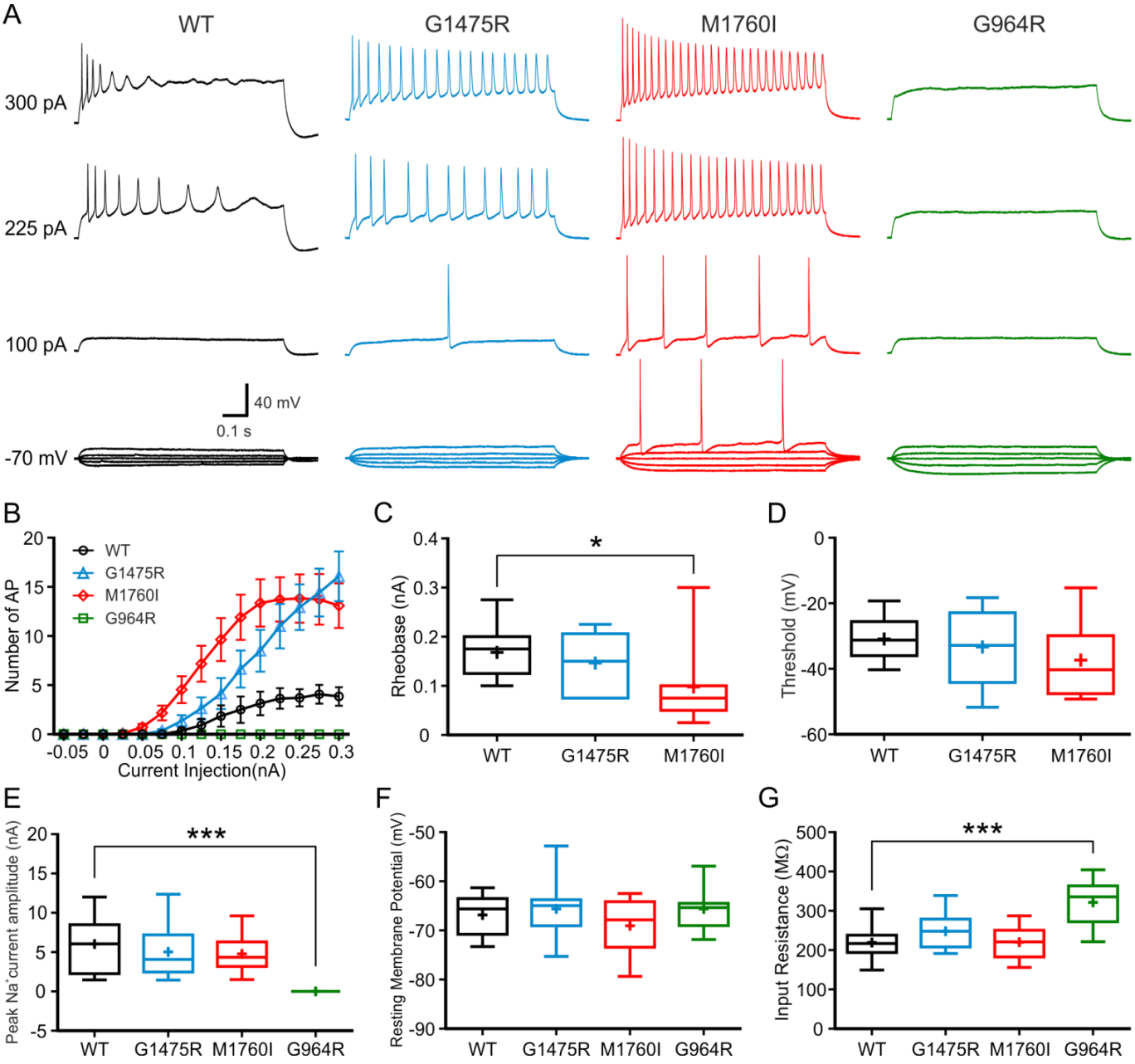

Supplementary Figure 7 Neuronal properties carried only by transfected WT or three more mutant channels. Hippocampal neurons were transfected with TTX-resistant WT or mutant $Na_V1.6$ channels. Neuronal properties were recorded in the presence of TTX to block all other endogenous voltage-gated Na^+ channels. (**A**) Representative traces of evoked APs recorded in the current clamp mode in neurons transfected with WT, G1475R, M1760I, or G964R channels, respectively. Neurons expressing G964R mutant channels under these conditions failed to fire APs. (**B**) Number of APs plotted versus injected current. Shown are means ± SEM for each data point (WT, n = 14; G1475R, n = 14; M1760I, n = 11; G964R, n =

11). The area under the curve was determined for each neuron over the whole range of current injections; the value for M1760I or G1475R mutant channels was significantly larger compared to WT channels. (**C**) Rheobase (minimal injected current to elicit an AP) of neurons transfected with WT or mutant channels. Transfections of M1760I mutant channels significantly reduced the rheobase compared to WT channels. (**D**) Thresholds of APs were not significantly different for WT and mutant channels. (**E**) Peak Na^+ current amplitude of neurons transfected with WT or mutant channels in the presence of TTX. The G964R mutation caused a complete loss of Na^+ current. (**F**) Resting membrane potentials were not significantly different between neurons transfected with WT or mutant channels. (**G**) Input resistance was enhanced by the G964R mutation compared to the WT but no change for other mutations. Box-and-whisker plots (**C**-**G**) show means (plus sign), the 25^{th}, 50^{th} and 75^{th} percentiles, minima and maxima; * $p < 0.05$; *** $p < 0.001$; one-way ANOVA with Dunnett´s posthoc test or ANOVA on ranks with Dunn´s posthoc test were performed.